ACS Catalysis

Research Article

pubs.acs.org/acscatalysis

Insight into the Deactivation of Au/CeO_2 Catalysts Studied by In Situ Spectroscopy during the CO-PROX Reaction

José A. Hernández,[†] Sergio A. Gómez,[‡] T. A. Zepeda,[*,§] Juan C. Fierro-González,[#] and Gustavo A. Fuentes[‡]

[†]Academia de Biotecnología y Farmacia, Unidad Profesional Interdisciplinaria de Ingeniería-Guanajuato (UPIIG-IPN), Silao, Guanajuato 07738, México

[‡]Departamento de Ingeniería Procesos e Hidráulica, Universidad A. Metropolitana-Iztapalapa, A.P. 55-534, México D.F. 09340, México

[§]Centro de Nanociencias y Nanotecnología- UNAM, Ensenada B.C., 22800, México

[#]Departamento de Ingeniería Química, Instituto Tecnológico de Celaya, Celaya, Guanajuato 38010, México

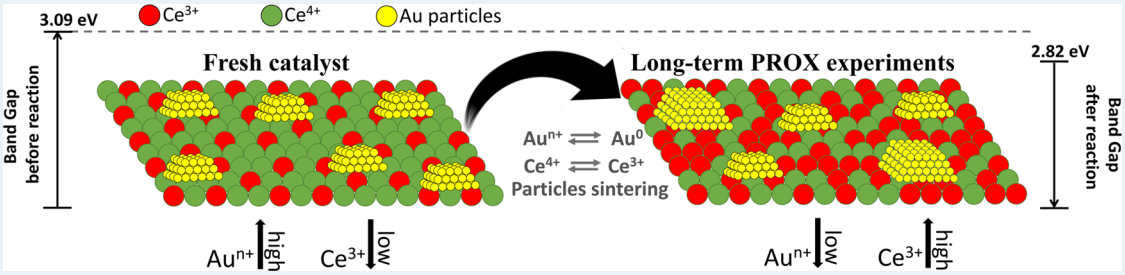

ABSTRACT: The activity and deactivation of Au/CeO_2 catalysts in the PROX reaction were measured during long-term experiments (TOS = 160 h) by in situ DRS-UV−vis spectroscopy. During the reaction, the support showed a decrease in band gap energy. The activity and selectivity to CO_2 were closely linked to the reduction of Au^{n+} species, the sintering of the reduced Au species, and to changes in the Ce^{3+}/Ce^{4+} ratio. This ratio increased during long-term PROX experiments, showing a decrement of surface oxygen atoms from the CeO_2 phase which participated in the reaction, after which the total oxygen fed to the reaction was wholly consumed. Also, almost all of the Au^{3+} species initially present in the catalysts were reduced to Au^{+} and Au^{0}. Results suggest that the activity loss is connected to the fast reduction of Au species and is also linked to changes in the redox properties of ceria, breaking the cycle that provides oxygen to the reaction. Sintering of the Au nanoparticles occurs in a longer time scale. On the other hand, in the case of fresh Au/CeO_2 catalysts, the Au^{n+}/Au^{0} ratio decreased with increasing Au content. This initial ratio affects CO_2 selectivity as a function of temperature.

KEYWORDS: *CO PROX, preferential CO oxidation, supported gold, deactivation, UV−vis spectra, band gap energy, surface plasmon*

1. INTRODUCTION

Given that H_2 management (storage and distribution) is very complex, the use of on-site reforming[1−5] to produce H_2 for fuel cells appears to be a logical alternative, albeit research is still needed to implement these options. The problem is to remove CO from H_2-rich streams, and to solve it a catalytic route is generally considered. This route consists in the selective oxidation inside a guard reactor of CO in an H_2-rich stream also containing H_2O and CO_2. A further constraint is that the reaction temperature during fuel cell operation should be close to 80 °C. So far, this reaction is possible with a limited number of noble metals, in particular, Pt, Pd, and Au.

Supported gold nanoparticles have received much attention after the group of Haruta[6,7] reported that they are extremely active in CO oxidation at low temperature. Since then, several reports have extensively reviewed the topic and suggested that the type of support, the pretreatment conditions, the catalyst preparation method, and the reaction conditions strongly influence catalyst activity and selectivity.[8−13] Catalysts are typically more active when gold particles are well dispersed on reducible metal oxides than on nonreducible metal oxides. This observation[14−16] has led some authors to conclude that the interaction between gold and the support is the determinant for catalytic activity, because a "synergic effect" occurs between the gold particles and the reducible metal oxides at the gold−support interface. This effect may involve redox processes, in which gold particles favor the reduction of the metal oxide, thus allowing lattice oxygen atoms from the support to become activated species available for the oxidation reactions.[14−16]

Gold catalysts must be highly active as well as resistant to deactivation during preferential CO oxidation (PROX reaction) to be competitive. Ideally, they should be stable during the estimated lifetime of fuel cells (~5000 h has been commonly assumed for mobile applications).[17] Because catalyst stability

Received: April 8, 2015
Revised: May 21, 2015
Published: May 22, 2015

DOI: 10.1021/acscatal.5b00739
ACS Catal. 2015, 5, 4003−4012

may depend on its resistance to undergo structural changes under reaction conditions, there is a motivation to identify the surface species that are necessary for the catalysts to be active. Some authors have reported that the interaction between Au nanoparticles and the support is the main reason for high catalytic activity. Others have stated that the presence of Au ions or metal Au nanoparticles plays a key role in the activity of Au catalysts during preferential oxidation of CO;[3,6,13,18,19] however, there is no general agreement yet.

A literature review indicates that deactivation trends during PROX depend on the gold content, the identity of the support, the composition of the reaction mixture, and the reaction conditions (different contact time expressed as W/Fco). Differences in catalysts and in reaction conditions during long-term PROX reaction tests complicate the comparison between reported results, making it unfeasible to assign the causes of deactivation to some specific changes or mechanisms. Nevertheless, deactivation of Au catalysts during PROX has been variously ascribed to the accumulation of carbonates, formation of hydroxyl groups, and sintering of Au nanoparticles,[3,17,20−22] among others. However, the observed deactivation and the assignment to one cause or another seems to depend mainly on the chosen reaction conditions and contact time, as well as on the characterization techniques.

In this work, CeO_2 was selected as support for the preparation of Au PROX catalysts. We performed long-term in situ DRS-UV−vis PROX reaction studies (TOS = 160 h), simultaneously analyzing the redox processes that occur on supported metals and on the supports themselves under reactive environments. The electronic environmental changes of the gold and cerium species were studied by XPS and XANES.

2. EXPERIMENTAL SECTION

2.1. Preparation of Au Catalysts Supported on CeO_2. Pure CeO_2 was obtained via thermal decomposition of $Ce(NO_3)_3{\cdot}6H_2O$ (Aldrich 99.99%) at 400 °C for 6 h. The supported Au catalysts were prepared by deposition−precipitation at room temperature,[27] using a support/deionized water ratio of 1 g/10 mL. A solution of $HAuCl_4{\cdot}3H_2O$ (Aldrich, ≥ 49% as Au) was dripped under strong stirring during 2 h. The pH was kept at 9.5 by the addition of a solution of NH_4OH (JT Baker, 0.1 M). The mixture was then aged at room temperature for 24 h. The solid was filtered and washed with 10 times the volume of deionized water used in the synthesis of the catalyst to remove chlorine ions. The solid was then dried at 125 °C for 2 h and finally calcined at 400 °C for 6 h in static air. The Au content was determined by atomic absorption. The labeling and Au loading of the catalysts is given in Table 1. The actual Au content was very close to the nominal Au loading.

2.2. Characterization Methods. The textural properties of all catalysts were determined from the adsorption−desorption isotherms of N_2, recorded with a Quantachrome Autosorb 1. Prior to the experiments, samples were degassed at 270 °C in vacuum for 5 h. Specific areas were calculated by applying the BET method to the N_2 adsorption data within the 0.005−0.25 P/P^0 range.[28,29] The average pore diameter was calculated by the Barret−Joyner−Halenda method (BJH) applied to the desorption branches of the N_2 isotherms. The cumulative pore volume was also obtained from the isotherms at P/P^0 = 0.99.

Catalysts were characterized by powder X-ray diffraction (step-scanning procedure; step size 0.02°; 0.5 s) with a Ragaku 2100 diffractometer using a monochromatic Cu Kα radiation (λ_{Cu} = 0.1541 nm) in the 2θ range between 2 and 80°.

Table 1. Nomenclature, Au Content, Textural Properties, and Mean Crystal Size of CeO_2 for Au/CeO_2 Fresh Samples

sample nomenclature	Au content[a] (% wt)	S_{BET} (m^2g^{-1})	Vp[c] (cm^3g^{-1})	Dp[d] (nm)	CeO_2 mean crystal size[b] (nm)
CeO_2	0.0	83	0.28	12.6	8.2
Au-24	0.24	112	0.33	12.9	8.39
Au-48	0.48	123	0.32	13.6	8.55
Au-74	0.74	97	0.35	13.8	8.75
Au-98	0.98	94	0.30	13.8	8.82
Au-124	1.24	86	0.30	13.7	8.97
Au-148	1.48	89	0.31	13.8	9.2
Au-174	1.74	87	0.24	13.3	9.31

[a]Determined by atomic absorption. [b]Calculated by using Scherrer's equation. [c]Vp = average pore volume. [d]Dp = average pore diameter.

The ex situ UV−vis diffuse reflectance spectra (DRS UV−vis) of the support and catalysts were recorded using a Cary 5E spectrophotometer equipped with a Praying Mantis diffuse reflection reaction cell (Harrick Scientific). All spectra were recorded at room temperature after heating the samples at 250 °C in He flow during 1 h. The spectrum of the support was subtracted from the spectrum of each catalyst.

X-ray photoelectron spectra of catalysts were measured in an A RIBER LDM-32 equipped with a hemispherical electron analyzer. A Mg Kα ($h\nu$ = 1253.6 eV) X-ray source was used. Each sample was first placed in a copper holder mounted on a sample-rod in the pretreatment chamber of the spectrometer, and it was then outgassed at 130 °C for 1 h before being transferred to the analysis chamber. All samples were outgassed at 10^{-5} mbar and then transferred to the ion-pumped analysis chamber. Pressure was kept below 7×10^{-9} mbar during data acquisition. The binding energies (BE) were referenced to the C 1s peak (284.9 eV) to account for charging effects. The areas of the peaks were computed after fitting the experimental spectra to Gaussian/Lorentzian curves and removal the background (Shirley function). Surface atomic ratios were calculated from the peak area ratios normalized by the corresponding atomic sensitivity factors.

The HR-TEM images of Au/CeO_2 catalysts were obtained using a JEOL-2100 microscope operated at 200 kV with a LaB_6 filament (resolution of 0.23 nm point) and equipped with an energy-dispersive-X-ray (EDX) instrument and a "Z" contrast detector. Each catalyst was crushed to a fine power, and a holey carbon film copper grid was dipped into the crushed powder.

Dispersive XANES spectra at the Au L_{III} edge were recorded at the X-ray beamline D06A-DXAS at the Brazilian Synchrotron Light National Laboratory (LNLS). The beamline was equipped with a curved Si (111) monochromator. Self-supporting wafers of the samples were placed in a stainless steel holder sealed with Kapton windows. XANES spectra were recorded in transmission mode with a cryogenically cooled CCD detector of 1340 × 1300 pixels. Each pixel has 20 × 20 μm^2 for a total image area of 26.8 × 26.0 mm^2. Conversion of data from pixel to energy was performed by comparing measurements of XANES spectra characterizing the reference gold foil. The energy step-size in the resulting spectra was approximately 0.3 eV. Data reduction and analysis was done with the software Athena.37. Au-L_{III} edge XANES spectra were calibrated with gold foil measured in transmission mode. The edge is represented as the inflection point of the first absorption

DOI: 10.1021/acscatal.5b00739
ACS Catal. 2015, 5, 4003−4012

peak at nearly 11919 eV. The exact value of the absorption edge for each spectrum was found by determining the maximum of the first derivative of the data in the region were the absorbance increased drastically. The data were normalized by dividing the absorption intensity by the height of the absorption edge.

2.3. Catalytic Activity Measurements. The activity of catalysts during the CO-PROX was measured in a quartz microreactor connected online to a GC Shimadzu 12-A with two packed columns (5-A and Porapack Q) and equipped with a TCD detector. The reactions were performance as a function of temperature at atmospheric pressure with a contact time W/Fco =158 g_{cat} h/mol CO. A mass of 80 mg of catalyst was placed in the microreactor, which was heated at 3 °C/min from room temperature to 400 °C. While heating, 100 mL/min of a mixture containing 1% CO, 1% O_2, 50% H_2, 48% N_2 (v/v) were flown through the reactor. Different catalytic tests were performed to determine the reaction conditions in which the activity changes were observable before the long-term experiments at a constant temperature of 80 °C. The conditions used during long-term experiments were W/F_{CO} = 8.6 g h/mol_{CO}, 25 mg of catalyst, and a flow rate of 153 cm^3/min of a gas mixture containing 1% CO, 1% O_2, 50% H_2 in N_2 at 80 °C. The use of a low W/Fco to evaluate the stability of Au/CeO_2 during long-term PROX is explained in the section 3 (Results and Discussion).

2.4. In Situ Diffuse Reflectance UV−vis Spectroscopy. The structural changes of catalysts were evaluated during PROX via in situ DRS UV−vis spectroscopy in a CARY/5E Varian spectrophotometer equipped with a diffuse reflectance reaction cell (Harrick Scientific). Spectra were measured from 1400 to 200 at 150 nm/min and a wavelength increment of 0.5 nm. Twenty-five milligrams of catalyst was used with a bed of 0.85 g of α-Al_2O_3. The reaction temperature was kept at 80 °C, and the same reaction mixture as well as W/F_{CO} were used during catalytic activity measurements (25 mg of catalyst, and a total flow of 153 cm^3/min of a gas mixture containing 1% CO, 1% O_2, 50% H_2 in N_2 at 80 °C).

3. RESULTS AND DISCUSSION

3.1. CO-PROX Activity during Programmed Temperature Reaction. Au/CeO_2 catalysts were highly active for both CO and H_2 oxidations at temperatures below 130 °C. The catalytic activity and selectivity dependent on both the Au content and the temperature are shown in Figure 1 and 2, respectively. As depicted in Figure 2, the catalysts increased their selectivity to CO_2 as the temperature was increased until a maximum in CO conversion was reached (Figure 1). H_2 oxidation was found to be dominant with a further temperature increase and depleted the limited amount of oxygen fed to the system (1% CO, 1% O_2, 50% H_2 in N_2).[30,31] In Figure 2, it is clear that the difference between high or low-Au-content catalysts, is the behavior of their selectivity with temperature. In general, at higher Au content, there was a lower light-off temperature for CO oxidation, and as a consequence, the maximum in CO conversion occurs at lower temperature. Changes in CO_2 selectivity with Au content and temperature suggest that CO adsorbs more strongly than hydrogen.[32]

3.2. CO-PROX Results during Long-Term Experiments. The stability of Au catalysts during PROX reported in the literature shows no common trend. This is in part caused by the use of different Au catalysts as well as by the different reaction conditions employed[3,5,17,31−41] (Table 2). A fact that has not been analyzed is the wide interval of W/Fco values that are

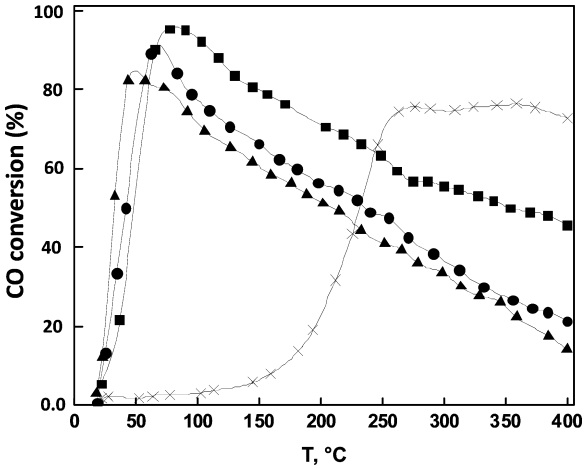

Figure 1. CO conversion versus reaction temperature during PROX over Au/CeO_2 catalysts. Reaction mixture: 1% CO, 1% O_2, 50% H_2, N_2 balance, contact time W/F_{CO} = 158 g_{cat} h/mol_{CO}. ■ Au-48; ● Au-98; ▲ Au-124, × pure CeO_2.

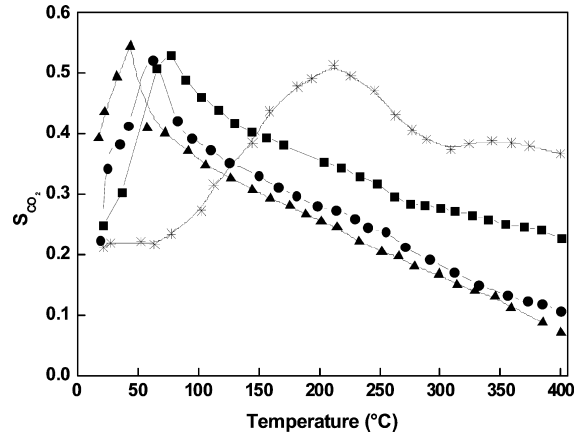

Figure 2. Selectivity to CO_2 versus reaction temperature during PROX over Au/CeO_2 catalysts. Reaction mixture: 1% CO, 1% O_2, 50% H_2, N_2 balance, contact time W/F_{CO} = 158 g_{cat} h/mol_{CO}. ■ Au-48; ● Au-98; ▲ Au-124, × CeO_2.

typically used. Even when they range from 8.6 to 220 g h/mol_{CO}, the initial CO conversion varies only from 0.63 to 0.99. W/F_{CO} value could be large enough that deactivation could be not detected during the first hours on stream of the reaction test. Also, as it was mentioned above, reaction tests at different temperatures have an effect on activity, selectivity, and deactivation. In fact, while some authors observed no deactivation,[5,31,39] others link deactivation to the presence of carbonates[40] and also to changes in Au^{n+} species[3,41] or in the support[17,40,41] as well (Table 2).

To determine an adequate W/F_{CO} range for long-term deactivation experiments, several reaction tests at 80 °C varying W/F_{CO} were performed. In Figure 3, the behavior of CO conversion vs W/F_{CO} at 80 °C for Au-48 (referred in the following to as low-Au-content catalyst) and Au-124 samples (referred in the following to as high-Au-content catalyst) are represented. The CO conversion vs W/F_{CO} curves for low and high Au content indicate low sensibility to the Au content (Figure 3). Both catalysts increase their CO conversion as W/F_{CO} was increased until W/F0 reached a value of 30 g_{cat} h/mol CO. At higher values, the CO conversion remains essentially constant for both samples. Thus, in order to properly observe

DOI: 10.1021/acscatal.5b00739
ACS Catal. 2015, 5, 4003−4012

Table 2. Comparison of Reaction Conditions Reported in the Literature during Long-Term PROX Studies

catalyst	Au (% wt)	T (°C)	W/Fco[c] (gh/mol_{CO})	feed composition (balance N_2)	TOS (h)	deactivation at 13 h[a] (%)	causes	ref
$Au/\alpha\text{-}Fe_2O_3$	2.3	80	33.4	1% CO, 1% O_2, 10% CO_2, 4% H_2O, 50% H_2	~17	27	presence of carbonates and changes in the support	7,27
Au/CeO_2	1	110	80.1	1% CO, 1% O_2, 2% CO_2, 2% H_2O, 40% H_2	48	0	ND[b]	26
$Au/\alpha\text{-}Fe_2O_3$	5	80	222.6	0.9% CO, 0.9% O_2, 22% CO_2, 4.7% H_2O, 50% H_2	~13	0	ND	23
Au/CeO_2-Ga or La	0.28	125	64.1	1% CO, 0.5% O_2, 15% CO_2, 10% H_2O, 50% H_2	50	0	reduction of Au species	5
Au/TiO_2	5	25	150.3	80 ppm of CO, 2% O_2, 2000 ppm of CO_2, 75% H_2	24	61	changes in species of Au^{n+}	3
Au/CeO_2–Co_3O_4	1	80	80.1	1% CO, 1% O_2, 50% H_2	300	9	reduction of Au^{n+} to Au^0 and Co_3O_4 to CoO	28
Au/CeO_2	0.48	80	8.6	1% CO, 1% O_2, 50% H_2	164	24	changes in species of	this work
Au/CeO_2	0.98	80	8.6	1% CO, 1% O_2, 50% H_2	164	49	Au^{n+} and in the redox	this work
Au/CeO_2	1.24	80	8.6	1% CO, 1% O_2, 50% H_2	164	61	cycle of CeO_2	this work

[a]Calculated from data reported in the literature. [b]ND = not determined. [c]W/Fco is the contact time expressed as g_{Cat}·h.$mol^{-1}{}_{CO}$.

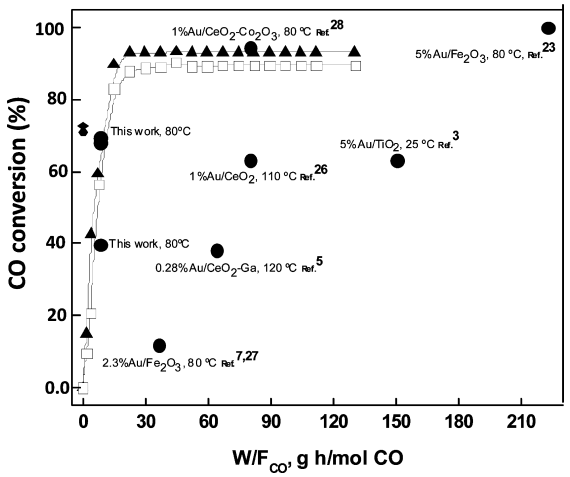

Figure 3. Behavior of CO conversion versus contact time (W/Fco) during PROX at 80 °C for Au-048 (▲), Au-098 (□), and data reported in the literature to study the deactivation of Au/catalysts during long-term PROX experiments (●).

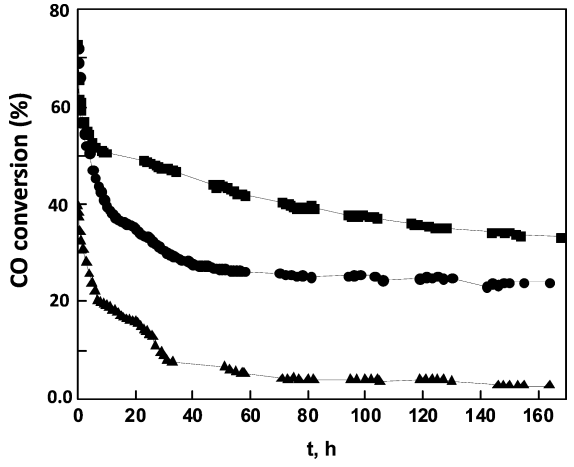

Figure 4. Deactivation patterns during PROX reaction at 80 °C over Au/CeO_2 catalysts using 1% CO, 1% O_2, 50% H_2, N_2 balance, contact time W/F_{CO} = 8.6 g_{cat} h/mol_{CO} and TOS = 164 h. ■ Au-48; ● Au-98; ▲ Au-124.

deactivation during long-term PROX experiments, it is necessary to operate the reactor at W/F_{CO} below 30 g_{cat} h/mol CO. For the long-term reaction test, W/F_{CO} = 8.6 g h/mol_{CO} was selected. Subsequently, 25 mg of catalyst and a flow rate of 153 cm^3/min of a gas mixture containing 1% CO, 1% O_2, 50% H_2 in N_2 at 80 °C were then used.

Figure 4 shows the performance of Au-48, Au-98, and Au-124 in the PROX reaction during 164 h on stream (TOS). During the first 10 h, there is a rapid deactivation of all catalysts tested. About 24% of the initial activity was lost during this stage. After 80 h of reaction, both Au-98 and Au-124 samples reached a pseudo stationary activity. The sample containing less Au gradually deactivated during 120 h of reaction. However, this sample showed the lowest catalytic deactivation under the reactions conditions employed. Deactivation results indicate that after 120 h of time-on-stream, the Au-48 sample has 49% of catalytic deactivation, whereas Au-98 and Au-124 samples have 66 and 95% of deactivation, respectively.

All catalysts had an initial selectivity to CO_2 of 55% (Figure 5). After 10 h of reaction, Au-48 had 50% of Sco_2 and remained

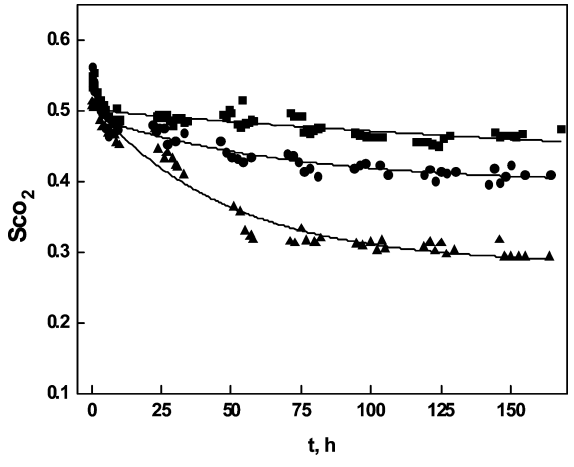

Figure 5. Selectivity to CO_2 during PROX at 80 °C over Au/CeO_2 catalysts using 1% CO, 1% O_2, 50% H_2, N_2 balance, contact time W/F_{CO} = 8.6 g_{cat} h/mol_{CO} and TOS = 164 h. ■ Au-48; ● Au-98; ▲ Au-124.

DOI: 10.1021/acscatal.5b00739
ACS Catal. 2015, 5, 4003−4012

almost constant during 160 h of TOS. Au-98 showed a similar behavior, but its Sco_2 was 44%. The higher Au content sample, Au-124, showed a decrease in its S_{CO2} during the first 60 h of reaction, and then it remained constant at 32% until the end of the experiment. Therefore, Sco_2 also depends on the Au content and on TOS. In order to explain those deactivation patterns, fresh and spent catalysts were characterized by ex situ DRS UV−vis and XPS. The deactivation was also followed during long-term PROX reaction via in situ DRS UV−vis spectroscopy in order to study the changes in Au species and Au nanoparticles as well as that of CeO_2 during long-term operation.

3.3. Characterization of Fresh and Used Catalysts. DRS UV−vis spectroscopy has been used extensively to study supported catalysts in order to obtain information on surface coordination as well as different oxidation states of metal ions by measuring d−d, f−d transitions and oxygen−metal ion charge transfer bands. All DRS UV−vis spectra of Au−ceria fresh catalysts have a band centered at 2.15 eV (Figure 6). This

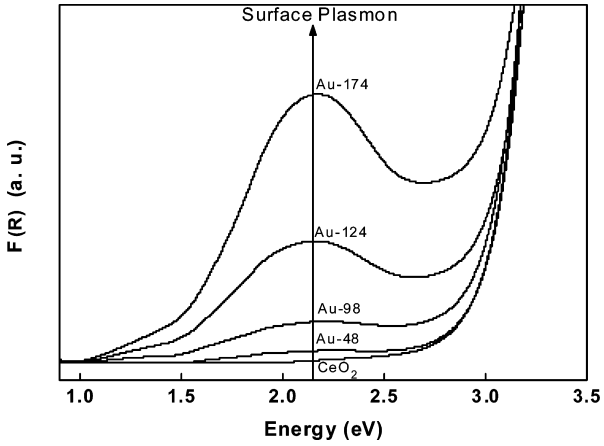

Figure 6. Evolution of the Au surface plasmon at 2.2 eV from ex situ DRS-UV−vis spectra of Au/CeO_2 fresh samples.

band is attributed to the surface plasmon (SP) resonance of Au nanoparticles. It arises from the collective oscillations of the free conduction band electrons induced by incident electromagnetic radiation with a wavelength greatly exceeding the particle diameter. SP resonance is a signature for the presence of metallic Au nanoparticles.[42,43] Results indicate that the intensity and the bandwidth of SP band increases gradually with the Au content (Figure 6), indicating the presence of Au^0 nanoparticles in fresh catalysts, and that their number and/or size increases with the Au content.[42−50] This was confirmed by HRTEM results, which confirmed that the particle size distribution changes with Au content. Mean particle sizes for Au-48, Au-98 and Au-124 fresh samples were 3.5, 8.2, and 10.2 nm, respectively (Figure 7).

On the other hand, all catalyst showed the Au $4f_{7/2}$ binding energies signals at 83.6, 84.5, and 85.6 eV in their XPS spectra (Figure 8). These signals are typical of metallic Au particles,

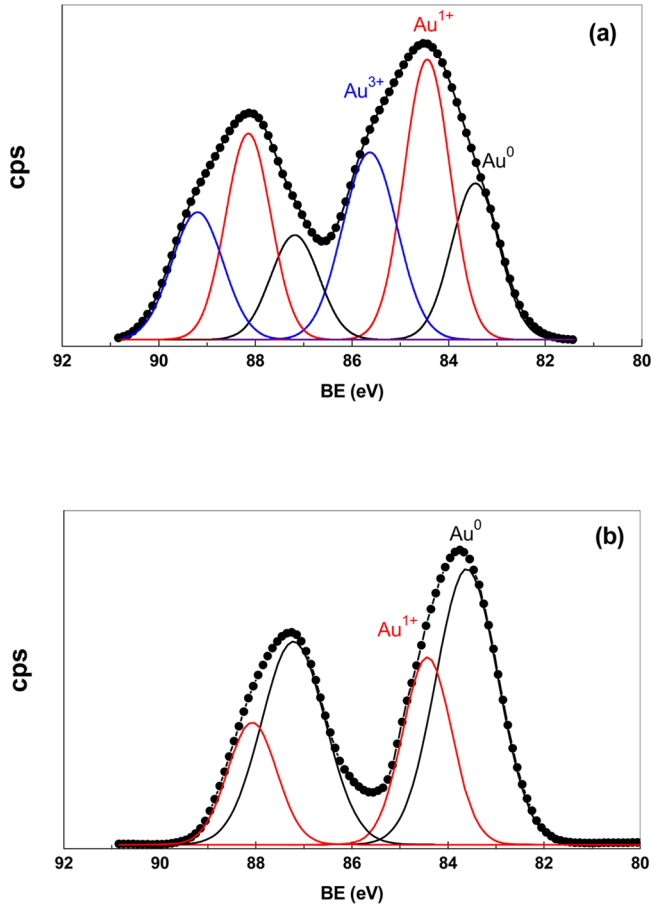

Figure 8. XPS spectra of Au-124 fresh sample (a) and after pretreatment with 15% H_2/N_2 for 1 h (b).

cationic Au^+ and Au^{3+} species, respectively.[47,48] After deconvolution of XPS spectra, we notice that as the Au content increases, both Au^{3+} and Au^0 fractions increase while the cationic Au^+ species decrease (Table 3). Samples having

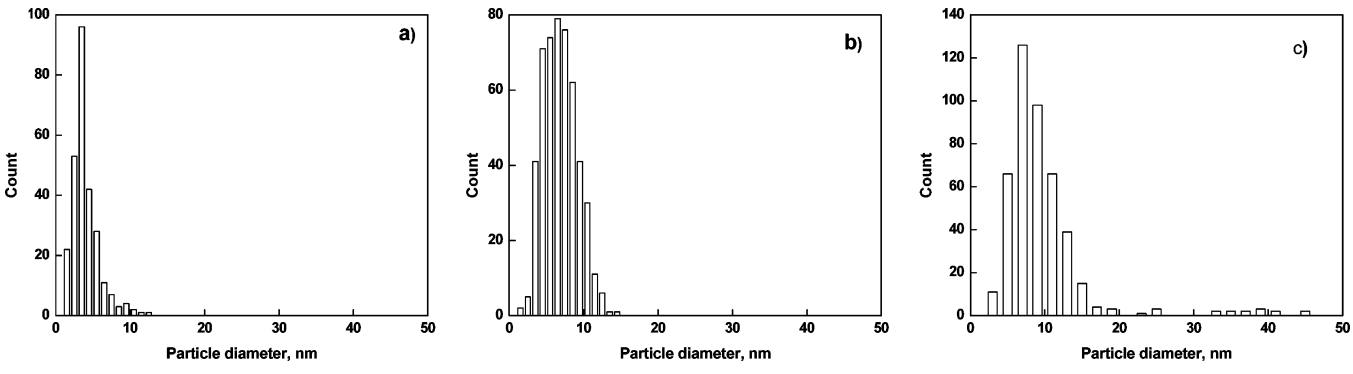

Figure 7. HR-TEM particle size distribution of Au/CeO_2 catalyst: (a) Au-48, (b) Au-98, and (c) Au-124 samples.

DOI: 10.1021/acscatal.5b00739
ACS Catal. 2015, 5, 4003−4012

Table 3. Binding Energies (eV) of Core Electrons of Ce 3d and Au 4f, Ce^{3+}/Ce^{4+},[a], Au/Ce, O/Ce and $Au^0/Au^{\delta+}$ Surface Atomic Ratios of Calcined Au/CeO_2 Samples

	Ce 3d							Au $4f_{7/2}$	Ce^{3+}/Ce^{4+},[a]	Au/Ce	O/Ce
catalyst	V	V′	V″	V‴	U	U″	U‴				
Au-048	822.4 (25%)	884.4 (15%)	886.5 (12%)	898.7 (9%)	902.0 (11%)	907.4 (8%)	917.1 (6%)	83.6 (7%)	0.41	0.019	1.59
								84.5 (82%)			
								85.6 (11%)			
Au-074	822.2 (24%)	884.5 (16%)	886.8 (12%)	898.7 (7%)	902.2 (11%)	907.5 (7%)	917.1 (7%)	83.6 (10%)	0.43	0.023	1.40
								84.5 (73%)			
								85.6 (17%)			
Au-098	822.1 (23%)	884.6 (17%)	886.7 (12%)	898.6 (9%)	902.1 (11%)	907.4 (7%)	917.3 (6%)	83.6 (16%)	0.46	0.038	1.19
								84.5 (64%)			
								85.6 (20%)			
Au-124	822.2 (22%)	884.5 (18%)	886.8 (11%)	898.7 (9%)	902.1 (12%)	907.4 (7%)	917.1 (5%)	83.6 (20%)	0.51	0.043	1.12
								84.5 (54%)			
								85.6 (26%)			

[a]The Ce^{3+}/Ce^{4+} ratio was calculated from XPS $Ce^{3+}/(Ce^{4+} + Ce^{3+})$ ratio; where, Ce^{3+} = (U′ + V′) and Ce^{4+} = (U + U″+ U‴ + V+ V″ + V‴).

low Au content show practically only cationic Au^{n+} species (82 and 11% of Au^+ and Au^{3+} species, respectively, and only 7% of Au^0), whereas the higher Au content sample has 20% of Au^0 and 54 and 26 of Au^+ and Au^{3+} species, respectively. The Au^0 and Au^{3+} atomic fractions (Table 3) follow the order: Au-124 > Au-98 > Au-74 > Au-48. From the DR UV−vis, HRTEM, and XPS results, it can be concluded that on fresh samples the amount of metallic Au^0 and Au^{3+} increases with the Au content. These results also indicate that the observed catalytic activity correlate with the amount of Au^{n+} species detected in fresh catalysts, i.e., the higher the Au^{n+} atomic fraction (n includes both $^{1+}$ and $^{3+}$ Au species), the higher the CO reaction rate during PROX at 80 °C at a steady state (Figure 9). This is the same trend than that reported by Guzman et al.[49] during the oxidation of CO.

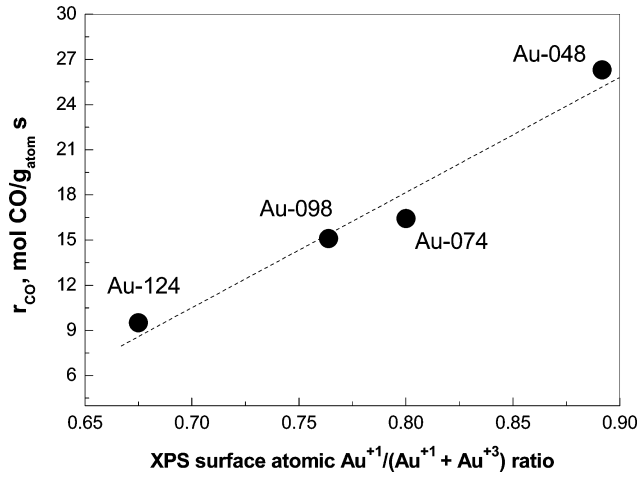

Figure 9. Relation between atomic Au^{n+} fraction and CO reaction rate during PROX at 80 °C at time on stream of 60 min (catalyst stabilization time).

DRS UV−vis spectra of fresh catalysts in the charge transfer region are presented in Figure 10. There are two principal absorption bands centered at 3.7 and 4.5 eV. The first absorption band is assigned to the electronic transition from oxygen to cerium III ($O^{2-} \rightarrow Ce^{3+}$), while the absorption band at 4.5 eV corresponds to the transition from oxygen to cerium IV ($O^{2-} \rightarrow Ce^{4+}$).[51,52] Both absorption bands are also affected

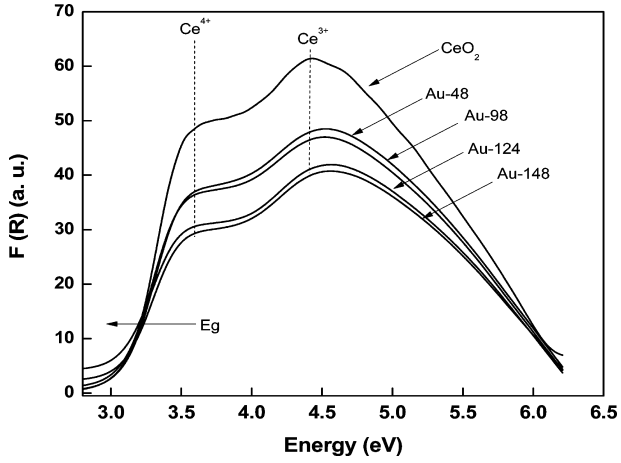

Figure 10. UV spectra for Au/CeO_2 fresh catalysts.

by the deposition of Au species. Besides the above, there is a change in the energy band gap (Eg) of cerium oxide after the deposition of Au. The band gap of ceria decreases with an increment in the Au content (from 3.2 to ∼3 eV in samples having higher Au content). This means that the presence of Au enhances slightly the electronic conduction in CeO_2. Also, the particle size of ceria, calculated by using the Scherrer's equation and the (1 1 1) XRD patterns, increases with the Au content (from 8.2 nm for CeO_2 to almost 9.3 nm for Au-124) (Table 1). The UV absorption edge wavelength is very sensitive to the particle size of semiconductor materials as in the case of ceria.[51] The changes observed in the band gap and in the mean crystal size of ceria with the Au content suggest that they are probably caused by changes in the Ce^{3+}/Ce^{4+} surface ratio (Ce^{4+} radius = 0.097 nm; Ce^{3+} radius = 0.114 nm) due to the interaction with Au species.[42,52−56] If an increment in the Au content changes the Ce^{3+}/Ce^{4+} surface ratio, this probably has also an important influence in the redox properties of CeO_2 and, as a consequence, in the catalytic activity.

XPS studies were performed in order to analyze the surface electronic environment of Ce ions and the nature of the surface Au species on catalysts before use. The binding energy (BE) values of the most intense Au $4f_{7/2}$ and Ce 3d core levels, Ce^{3+}/Ce^{4+}, Au/Ce, and O/Ce surface atomic ratios are listed in Table 3. XPS Ce 3d signals of catalysts show eight peaks corresponding to the spin−orbit doublet (SOD) and satellite

DOI: 10.1021/acscatal.5b00739
ACS Catal. 2015, 5, 4003−4012

lines characteristic of Ce in oxidized state.[57−60] As an example, the XP spectrum on Au-124 sample is shown in Figure 11. The

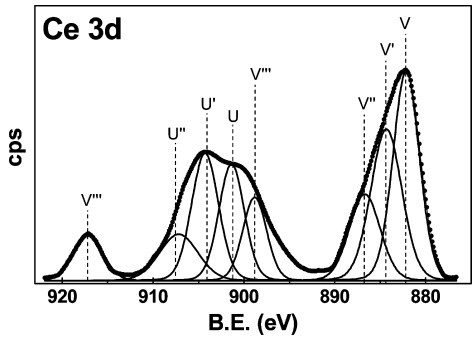

Figure 11. XPS spectra of the Ce 3d core electron levels for Au-124 catalyst.

lower Ce^{3+}/Ce^{4+} surface ratio was observed in the Au-48 sample (Ce^{3+}/Ce^{4+} atomic ratio of 0.41) (Table 3). The surface Ce^{3+}/Ce^{4+} ratio follows the order: Au-48 < Au-74 < Au-124. As the Au content increases, there is also an increase in the electronic conduction of ceria (change in ceria band gap), which is related to the observed increase in Ce^{3+}/Ce^{4+} ratio and in the mean crystal size of ceria (Figure 12). These changes depend on the proportion of Au^{o} and Au^{n+} species, which in turn depend on the Au content in the catalyst.

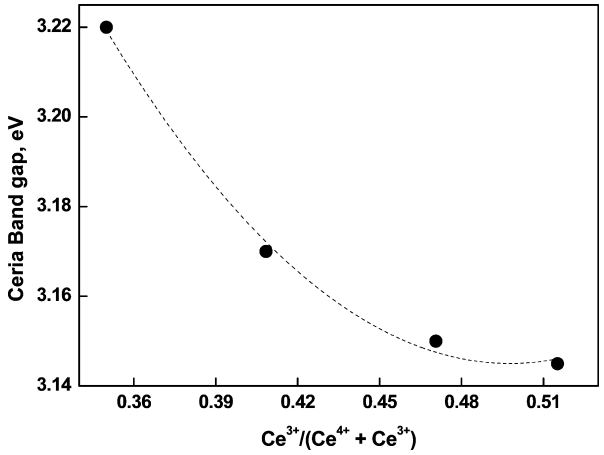

Figure 12. Relation between Ce^{3+}/Ce^{4+} ratio and band gap energy of ceria in catalysts fresh.

The O/Ce ratio decreases when the Ce^{3+}/Ce^{4+} ratio increases, this is due to a change in the Ce^{3+} content, and therefore, the surface oxygen decreases. A decrease in the surface O/Ce ratio has a negative effect on the CO reaction rate, probably because there is a smaller supply of oxygen. Additionally, we observed a strong impact of cationic Au species on the reaction rate. An increment in the Au^{0} fraction results in a decrement in the CO reaction rate. The catalytic behavior observed could be related to the Ce^{3+}/Ce^{4+} and Au^{n+}/Au^{o} surface ratios, which are associated with the surface oxygen mobility.

3.4. Evidence of Reduction of Au Species and Over-Reduction of Ceria via In Situ UV−vis Reaction. In order to understand deactivation of our catalysts, we measured in situ DRS UV−vis spectra at the same reaction conditions used in section 3.3 for each catalyst. Figure 13 shows the electronic

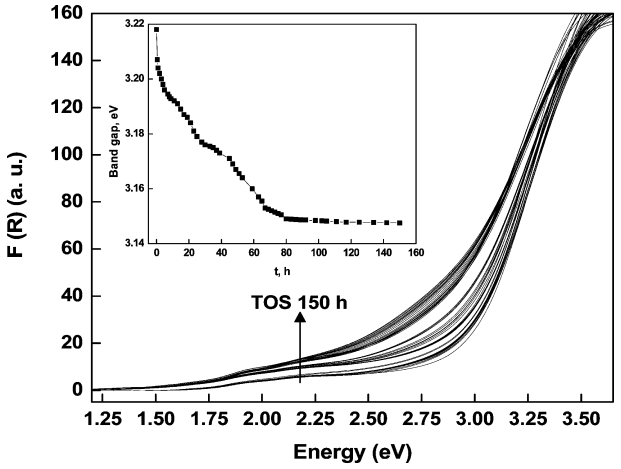

Figure 13. Electronic spectra during the in situ PROX reaction over Au-48 catalyst at 80 °C with 1% CO, 1% O_2, 50% H_2, N_2 balance, contact time W/F_{CO} = 8.6 g_{cat} h/mol_{CO} and TOS = 150 h.

spectra during the in situ experiments for sample Au-48. The intensity of the Au SP band slightly increases during the PROX reaction. The Au size effect on the SP absorption has been linked to the SP bandwidth, which decreases when the particle size increases. It has been established that the bandwidth is inversely proportional to the radius of the particles for sizes smaller than those about 20 nm when they form colloidal solutions.[42,45,48,61−63] For larger Au particles in solution, SP bandwidth increases with the particle size. Our deactivation results indicate that reduction and a slight sintering of Au species occur during long-term reaction.

A significant decrease in ceria band gap, from 3.09 to 2.82 eV, occurred during reaction (inset in Figure 13). The change in ceria band gap with TOS tracks the CO PROX deactivation of low-Au-content catalyst (Figure 4). This is an indication that there are also important changes in the electronic properties ceria during PROX reaction.

Figure 14 shows the evolution of the in situ electronic spectra for Au-98 sample during 150 h of PROX reaction. Also, as in the case of low Au content, the SP bandwidth of Au-98 decreases from 0.49 to 0.41 eV, and its intensity increases during reaction, indicating again reduction and sintering of Au

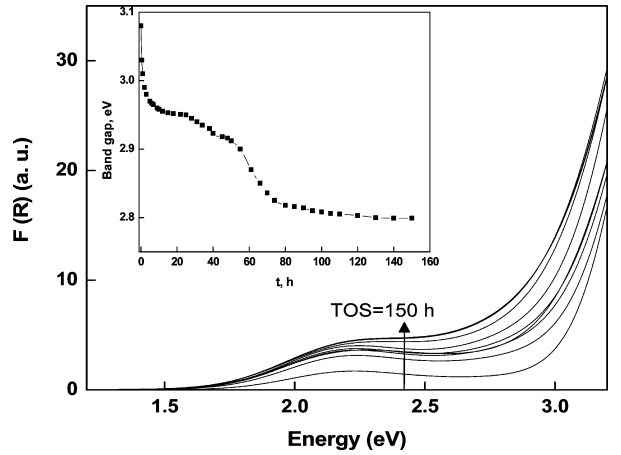

Figure 14. Electronic spectra during the in situ PROX reaction over Au-98 catalyst at 80 °C with 1% CO, 1% O_2, 50% H_2, N_2 balance, contact time W/F_{CO} = 8.6 g_{cat} h/mol_{CO} and TOS = 150 h.

DOI: 10.1021/acscatal.5b00739
ACS Catal. 2015, 5, 4003−4012

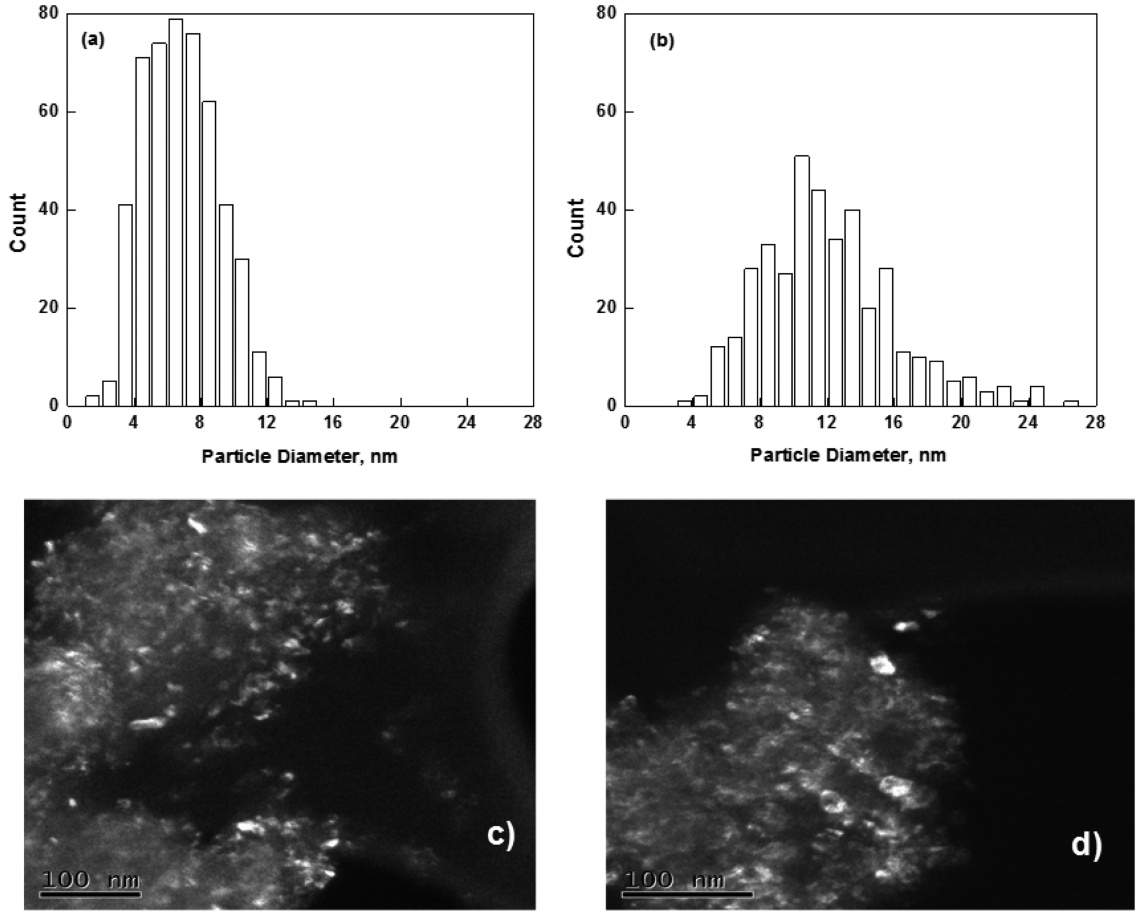

Figure 15. Particle size distribution of Au-98 sample (Au/CeO_2 with 0.98 Au wt %) for the following: (a) fresh sample, (b) after PROX for 160 h and HR-TEM images of Au nanoparticles for (c) fresh sample and (d) after PROX for 160 h.

species. This increment is more evident than that observed in the low-Au-content sample, which indicates an increase in concentration and size of the supported Au nanoparticles.[42,61−64] Results suggest that the Au reduction occurs during the first 10 h on stream, and after that, the sintering of Au nanoparticles occurs. In fact, TEM results (Figure 15) clearly indicate the occurrence of a sintering process of Au nanoparticles during reaction. The average Au particle size after reaction also depends on the Au content and on the time on stream.

We can notice that in Au-98 sample changes also occur in the ceria band gap, from 3.07 to 2.78 eV, during reaction (inset in Figure 14). Again the behavior of ceria band gap versus TOS is similar to the deactivation curve (Figure 4). In situ DRS-UV−vis results indicate that during deactivation of low and high content of Au content catalysts during PROX reaction, Au reduction and a decrease in CeO_2 band gap occurred.

Taking into account DRS UV−vis and XPS results on fresh catalysts, the Ce^{3+}/Ce^{4+} ratio, and the observed changes in CeO_2 band gap during deactivation, the amount of Ce^{3+} should then increase during deactivation due to the reducing environment in the PROX reaction (feed gas mixture composition: 1% CO, 1% O_2, 50% H_2 in N_2). This means that an over-reduction of CeO_2 occurred during reaction. Zacl et al.[65] have reported that the problem of deactivation is likely to be universal for all noble metal/ceria system in which a significant fraction of hydrogen in the feed creates a reducing environment facilitates the over-reduction of the support. Recently, Jimenez-Lam et al.[66] used an in situ dispersive XANES probe to determine that in the case of Au/Fe_2O_3 the reduced gold provides sites for H_2 adsorption and dissociation, which is then spillover from the gold to the support, favoring its reduction and restructuring. Our results for Au/CeO_2 seem to agree with those of Jimenez-Lam et al.[66] At high Au content, the amount of Au^0 nanoparticles is higher and the loss in activity is greater than that observed with low-Au-content catalyst. In the case of PROX, the high amount of H_2 in the feed helps to the fast reduction of Au and then reduced Au nanoparticles helps to over-reduce the ceria. In order to probe this, the sample Au-124 was pretreated at 150 °C using 30 cm^3/min of a 15% H_2 in N_2 for 1 h, and the XPS spectra of both Au and Ce was measured. The Au XPS spectrum indicate that after this treatment all Au^{3+} species present in the fresh calcined sample (Table 3) were reduced to Au^0; after 1 h of reduction, the atomic fractions of Au^0 and Au^{1+} were 0.7 and 0.3, respectively (Figure 8). This indicates that the reduction of Au^{n+} species occurs under PROX reaction conditions. XANES spectra of fresh and used samples also indicate that under PROX conditions, the reduction of Au species is a very fast process (Figure 16). Also, Ce XPS spectrum of the pretreated Au-124 sample indicates an increase of 0.9% in the Ce^{3+}/Ce^{4+} atomic ratio, with respect to the fresh calcined sample (Table 3). Thus, the results indicate that reduction of Au^{3+} species, changes in Ce^{3+}/Ce^{4+} atomic ratio and sintering are involved in deactivation of Au/CeO_2 PROX catalysts.

DOI: 10.1021/acscatal.5b00739
ACS Catal. 2015, 5, 4003−4012

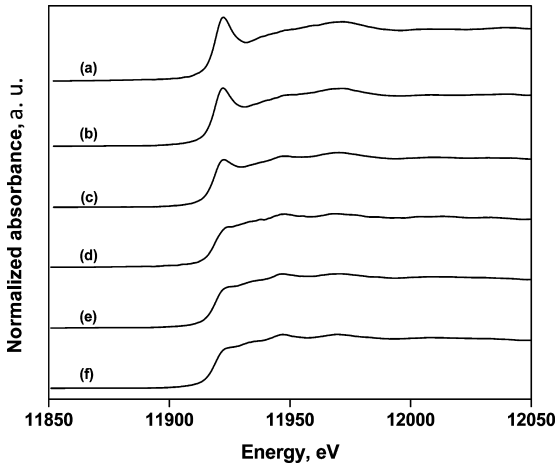

Figure 16. Spectra XANES of Au/CeO_2 catalysts: fresh (a) 0.24 Au wt %, (b) 0.74 Au wt %, (c) 1.5 Au wt % and after 160 h in PROX to 80 °C (d) 0.24 Au wt %, (e) 0.74 Au wt %, and (f) 1.5 Au wt %.

4. CONCLUSIONS

At higher Au content, there was a lower light-off temperature for CO oxidation. The stability of low-Au-content catalysts (Au-48 sample with 0.48 Au wt %) during PROX is higher than those catalysts with higher Au content. After a TOS of 160 h, only the selectivity to CO_2 of low-Au-content catalysts remained almost at 50%. Deactivation patterns show a particular trend. There is a fast deactivation between the first 10 h of PROX reaction. All catalysts lost around 24% of their initial activity after 10 h on stream. Then a slow activity decay process occurs until a pseudo stationary activity is reached at TOS = 80−120 h. Characterization results of fresh samples indicate that the structural, electronic, and catalytic properties of Au/CeO_2 depend on Au content. Our analysis of Au/CeO_2 catalysts shows the presence of Au^0, Au^{1+}, and Au^{3+} species. They were identified on the basis of DRS UV−vis and XPS spectra of catalysts before and after reaction. Samples having low Au content show practically 93% of cationic Au^{n+} species, whereas the high-Au-content sample (Au-124 sample with 1.24 Au wt %) has 20% of Au^0. By using in situ DRS in the UV−vis region, we were able to follow the behavior of Au nanoparticles and the changes in the band gap of CeO_2 in order to relate those observations to the catalytic stability of the Au/CeO_2 during long-term PROX experiments. Deactivation of Au/CeO_2 during PROX is related to (i) the reduction of the cationic Au species, (ii) sintering of Au nanoparticles, and (iii) the surface reduction of CeO_2. It appears that deactivation is caused mainly by an alteration of the redox cycle of ceria, which is caused by the reduction of Au species affecting the availability of oxygen. These results help to explain the changes observed during deactivation of Au/CeO_2 catalysts.

AUTHOR INFORMATION

Corresponding Author

*E-mail: trino@cnyn.unam.mx (T.A.Z.).

Notes

The authors declare no competing financial interest.

ACKNOWLEDGMENTS

The authors are grateful to E. Flores, E. Aparicio, D. Dominguez, J.A. Díaz, F. Ruiz, and I. Gradilla for their technical assistance. J.A.H. acknowledges Consejo Nacional de Ciencia y Tecnología (CONACyT) for a Scholarship (203299). T.AZ. acknowledges the financial support of CONACyT (Projects 152012 and 117373) and UNAM (Proyect PAPIIT IA200914). S.A.G. acknowledges the financial support of CONACyT (Project 42292) and the Laboratorio Nacional de Luz Sincrotron, Campinas, Brasil.

REFERENCES

(1) Crabtree, G. W.; Dresselhaus, M. S.; Buchanan, M. V. *Phys. Today* **2004**, *57*, 39−45.
(2) Moreno, M.; Baronetti, G. T.; Laborde, M. A.; Mariño, F. J. *Int. J. Hydrogen Energy* **2008**, *33*, 3538−3542.
(3) Steyn, J.; Pattrick, G.; Scurrell, M. S.; Hildebrandt, D.; Raphulu, M. C.; van der Lingen, E. *Catal. Today* **2007**, *122*, 254−259.
(4) Ogden, J. M. *Phys. Today* **2002**, *55*, 69−74.
(5) Deng, W.; De Jesús, J.; Saltsburg, H.; Flytzani-Stephanopoulos, M. *Appl. Catal., A* **2005**, *291*, 126−135.
(6) Haruta, M.; Tsubota, S.; Kobayashi, T.; Kageyama, H.; Genet, M. J.; Delmon, B. *J. Catal.* **1993**, *144*, 175−192.
(7) Haruta, M.; Kobayashi, T.; Sano, H.; Yamada, N. *Chem. Lett.* **1987**, *16*, 405−408.
(8) Bond, G. *Gold Bulletin* **2001**, *34*, 117−119.
(9) Hernández, J. A.; Gómez, S.; Pawelec, B.; Zepeda, T. A. *Appl. Catal., B* **2009**, *89*, 128−136.
(10) Kandoi, S.; Gokhale, A. A.; Grabow, L. C.; Dumesic, J. A.; Mavrikakis, M. *Catal. Lett.* **2004**, *93*, 93−100.
(11) Bond, G.; Thompson, D. T.; Louis, C. *Catalysis by Gold, Catalytic Science Series*; Imperial College Press: London, 2006; Vol. *6*, p 280, pp 1−384.
(12) Solsona, B.; Conte, M.; Cong, Y.; Carley, A.; Hutchings, G. *Chem. Commun.* **2005**, *18*, 2351−2353.
(13) Enache, D. I.; Edwards, J. K.; Landon, P.; Solsona-Espriu, B.; Carley, A. F.; Herzing, A. A.; Watanabe, M.; Kiely, C. J.; Knight, D. W.; Hutchings, G. J. *Science* **2006**, *311*, 362−365.
(14) Haruta, M. *Stud. Surf. Sci. Catal.* **2002**, *144*, 115−121.
(15) Bond, G. C. *Catal. Today* **2002**, *72*, 5−9.
(16) Hutchings, G. *J. Gold Bull.* **1996**, *29*, 123−130.
(17) Minico, S.; Scire, S.; Crisafulli, C.; Visco, A. M.; Galvagno, S. *Catal. Lett.* **1997**, *47*, 273−276.
(18) Chang, C. K.; Chen, Y. J.; Yeh, C. *Appl. Catal., A* **1998**, *174*, 13−23.
(19) Hutching, G. J.; Hall, M. S.; Carley, A. F.; Landon, P.; Solsona, B. E.; Kiely, C. J.; Herzing, A.; Makke, M.; Moulijn, J. A.; Overweg, A.; Fierro-González, J. C.; Guzmán, J.; Gates, B. C. *J. Catal.* **2006**, *242*, 71−81.
(20) Schubert, M. M.; Plzak, V.; Garche, J.; Behm, R. J. *Catal. Lett.* **2001**, *76*, 143−150.
(21) Costello, C. K.; Yang, J. H.; Law, H. Y.; Wang, Y.; Lin, J.-N.; Marks, L. D.; Kung, M. C.; Kung, H. H. *Appl. Catal., A* **2003**, *243*, 15−24.
(22) Haruta, M. *Catal. Today* **1997**, *36*, 153−166.
(23) Kozlov, A. I.; Kozlova, H.; Asakura, K.; Matsui, Y.; Kogure, T.; Shido, T.; Iwasawa, Y. *J. Catal.* **2000**, *196*, 56−65.
(24) Aguilar Guerrero, V.; Gates, B. C. *Chem. Commun.* **2007**, *14*, 3210−3212.
(25) Lui, Y.; Fu, Q.; Stephanopoulos, M. F. *Catal. Today* **2004**, *241*, 93−95.
(26) Trovarelli, A. *Catal. Rev.: Sci. Eng.* **1999**, *38*, 439−444.
(27) Trovarelli, A. *Catalysis by Ceria and Related Materials, Catalytic Science Series*; Imperial College Press: London, 2002; Vol. *2*, p 53, pp 51−83.
(28) Deetlefs, M.; Raubenheimer, H. G.; Esterhuysen, M. W. *Catal. Today* **2002**, *72*, 29−41.
(29) Barret, E. P.; Joyner, L. J.; Halenda, P. P. *J. Am. Chem. Soc.* **1951**, *73*, 373−380.
(30) Haruta, M.; Yamada, N.; Kobayashi, T.; Iijima, S. *J. Catal.* **1989**, *115*, 301−309.

DOI: 10.1021/acscatal.5b00739
ACS Catal. 2015, 5, 4003−4012

(31) Landon, P.; Ferguson, J.; Solsona, B. E.; García, T.; Carley, A.; Herzing, A. A.; Kiely, J.; Golunski, S. E.; Hutchings, G. *Chem. Commun.* **2005**, *27*, 3385−3387.
(32) Xu, J.; Li, P.; Song, X.; Qi, Z.; Yu, J.; Yuan, W.; Han, Y. *Ind. Eng. Chem. Res.* **2010**, *49*, 4149−4155.
(33) Bond, G.; Thompson, D. T.; Louis, C. *Catalysis by Gold, Catalytic Science Series*; Imperial College Press: London, 2006; Vol. *6*, p 84, pp 1−384.
(34) Ilieva, L.; Pantaleo, G.; Ivanov, I.; Maximova, I.; Zanella, R.; Kaszkur, Z.; Venezia, A. M.; Andreeva, D. *Catal. Today* **2010**, *158*, 44−55.
(35) Liotta, L. F.; Di Carlo, G.; Pantaleo, G.; Venezia, A. M. *Catal. Today* **2010**, *158*, 56−62.
(36) Ayastuy, J.; Gurbani, A.; González Marcos, M.; Gutiérrez Ortiz, M. *Int. J. Hydrogen Energy* **2010**, *35*, 1232−1244.
(37) Mariño, F.; Descorme, C.; Duprez, D. *Appl. Catal., B* **2004**, *54*, 59−66.
(38) Sedmak, G.; Hočevar, S.; Levec, J. *J. Catal.* **2003**, *213*, 135−150.
(39) Rodríguez, J. A. *Catal. Today* **2010**, *160*, 3−10.
(40) Luengnaruemitchai, A.; Osuwan, S.; Gulari, E. *Int. J. Hydrogen Energy* **2004**, *29*, 429−435.
(41) Schubert, M. M.; Venugopal, A.; Kahlich, M. J.; Plzak, V.; Behm, R. J. *J. Catal.* **2004**, *222*, 32−40.
(42) Wang, H.; Zhu, H.; Qin, Z.; Liang, F.; Wang, G.; Wang, J. *J. Catal.* **2009**, *264*, 154−162.
(43) Link, S.; El-Sayed, M. A. *J. Phys. Chem. B* **1999**, *103*, 8410−8426.
(44) Zanella, R.; Giorgio, S.; Shin, C.-Ho; Henry, C. R.; Louis, C. *J. Catal.* **2004**, *222*, 357−367.
(45) Kreibig, U.; Genzel, L. *Surf. Sci.* **1985**, *156*, 678−700.
(46) Pestryakov, A. N.; Lunin, V. V.; Kharlanov, A. N.; Bogdanchikova, N. E.; Tuzovskaya, I. V. *Eur. Phys. J. D* **2003**, *24*, 307−309.
(47) Bensalem, A.; Muller, J. C.; Bozon Verduraz, F. *J. Chem. Soc., Faraday Trans.* **1992**, *88*, 153−154.
(48) Veith, G. M.; Lupini, A. R.; Pennycook, S. J.; Ownby, G. W.; Dudney, N. J. *J. Catal.* **2005**, *231*, 151−158.
(49) Peza-Ledesma, C. L.; Escamilla-Perea, L.; Nava, R.; Pawelec, B.; Fierro, J. L. G. *Appl. Catal., A* **2010**, *375*, 37−48.
(50) Guzman, J.; Carrettin, S.; Corma, A. *J. Am. Chem. Soc.* **2005**, *127*, 3286−3287.
(51) Fu, Q.; Saltsburg, H.; Flytzani-Stephanopoulos, M. *Science* **2003**, *301*, 935−938.
(52) Ranga Rao, G.; Sahu, H. Ranjan *Proc. - Indian Acad. Sci., Chem. Sci.* **2001**, *113*, 651−658.
(53) Li, R.; Yabe, S.; Yamashita, M.; Momose, S.; Yoshida, S.; Yin, S.; Sato, T. *Mater. Chem. Phys.* **2002**, *75*, 39−44.
(54) Zhang, Y. W.; Si, R.; Liao, C. S.; Yan, C. H.; Xiao, C. X.; Kou, Y. *J. Phys. Chem. B* **2003**, *107*, 10159−10167.
(55) Wang, Z.; Quan, Z.; Lin, J. *Inorg. Chem.* **2007**, *46*, 5237−5242.
(56) Liao, X.; Chu, W.; Dai, X.; Pitchon, V. *Appl. Catal., A* **2012**, *449*, 131−138.
(57) Ho, C.; Yu, J. C.; Kwong, T. A.; Mak, C.; Lai, S. *Chem. Mater.* **2005**, *17*, 4514−4522.
(58) Burroughs, P.; Hamnett, A.; Orchard, A. F.; Thornton, G. *J. Chem. Soc., Dalton Trans.* **1976**, *17*, 1686−1691.
(59) Fonseca, J.; Royer, S.; Bion, N.; Pirault-Roy, L.; Rangel, M. C.; Duprez, D.; Epron, F. *Appl. Catal., B* **2012**, *128*, 10−20.
(60) Scirè, S.; Crisafulli, C.; Roccobene, P. M.; Patanè, G.; Pistone, A. *Appl. Catal., A* **2012**, *66*, 417−418.
(61) Zou, Z. Q.; Meng, M.; Guo, L. H.; Zha, Y. Q. *J. Hazard. Mater.* **2009**, *163*, 835−842.
(62) Link, S.; El Sayed, M. A. *Annu. Rev. Phys. Chem.* **2003**, *54*, 331−366.
(63) Da Silva Lima Fonseca, J.; Ferreira, H. S.; Bion, N.; Pirault-Roy, L.; Rangel, M. C.; Duprez, D.; Epron, F. *Catal. Today* **2012**, *180*, 34−41.
(64) Maaza, M.; Nemraoui, O.; Sella, C.; Beye, A. C. *Gold Bull.* **2005**, *38*, 100−106.
(65) Zalc, J. M.; Sokolovskii, V.; Löffler, D. G. *J. Catal.* **2002**, *206*, 169−171.
(66) Jiménez-Lam, S. A.; Cárdenas-Galindo, M. G.; Handy, B. E.; Gomez, S. A.; Fuentes, G. A.; Fierro-González, J. C. *J. Phys. Chem. C* **2011**, *115*, 23519−23526.

DOI: 10.1021/acscatal.5b00739
ACS Catal. 2015, 5, 4003−4012